# Deep melting and sodic metasomatism underneath the highly oblique-spreading Lena Trough (Arctic Ocean)

Eric Hellebrand *, Jonathan E. Snow

*Max-Planck-Institut für Chemie, Postfach 3060, 55020 Mainz, Germany*

## Abstract

Abyssal peridotites collected along the highly oblique-spreading Lena Trough north of Greenland and Spitsbergen have mineral compositions that are similar to residual abyssal peridotites, except for high sodium concentrations in clinopyroxene (cpx). Most samples are lherzolites with light rare earth element (REE)-depleted cpx trace element patterns, but significantly fractionated middle to heavy REE ratios at relatively high heavy REE concentrations. Such characteristics can only be explained by initial melting of a garnet peridotite followed by low degrees of melting in the stability field of spinel peridotite. The residual garnet signature requires either a high potential temperature of the upwelling mantle, or elevated solidus-lowering water contents. The limited spinel field melting suggests a deep cessation of melt extraction, possibly because of the presence of a thick lithospheric cap. This is consistent with the extremely low effective spreading rate and the vicinity to a passive continental margin, which allow conductive cooling to reach deeper levels than commonly estimated for faster mid-ocean ridges. High sodium concentrations in cpx are neither explainable by melt refertilization, nor by a simple diffusion mechanism. The efficient fractionation of sodium from the light REE requires post-melting metasomatism, which is typically restricted to the subcontinental lithosphere. This might imply that the Lena Trough peridotites represent unroofed subcontinental mantle, from which no melt was extracted during the opening of the Lena Trough. It is more likely that sodic metasomatism occurred after partial melting underneath the Lena Trough, and that such an enrichment process is responsible for elevated sodium concentrations in abyssal peridotites elsewhere. Sodium in cpx of residual peridotites can therefore not serve as an indicator of partial melting or melt refertilization.
© 2003 Elsevier B.V. All rights reserved.

*Keywords:* abyssal peridotite; partial melting; melt–rock reaction; metasomatism; secondary ion mass spectrometry

## 1. Introduction

Peridotite occurs on the ocean floor in a variety of tectonic settings. In addition to being found on the walls of oceanic transform faults [1,2], lower crustal and mantle rocks are now known to be abundant on megamullion surfaces (usually near transforms) [3,4], magmatically starved sections of normally rifted ridges [5,6] and on amagmatic passive continental margins [7,8]. A newly recognized type of plate boundary where peridotites play a major role occurs at slow-spreading rates

* Corresponding author. Tel.: +49-6131-305-220; Fax: +49-6131-371-051.
  *E-mail address:* ehelle@mpch-mainz.mpg.de (E. Hellebrand).

where the preferred failure direction of the crust re-orients itself to follow the plate boundary [9], rather than breaking up into the classic orthogonal rift/transform stairstep geometry, as observed in most transform-dominated regions.

The Lena Trough (Fig. 1), located at the smallest distance between North America and Eurasia, is an example of an oblique-spreading plate boundary. The Lena Trough basement is closer to continental margin than the nearby amagmatic Molloy Ridge, and could be made of thinned, rifted continental crust, or mid-ocean ridge lithologies. Dredging at the small Molloy Ridge segment south of Lena Trough has yielded exclusively serpentinized mantle peridotites [10], similar to the West Iberian margin.

Such near-continental large-scale exposures of serpentinized mantle rocks are known from fossil ocean–continent transitions (OCTs). These non-volcanic rifted margins have been the subjects of numerous geophysical and geological surveys in the past two decades. Most investigations focused on the West Iberian margin. Here, the most prominent feature is a ~100 km wide continuous belt of serpentinized peridotite parallel to the margin of Iberia ([11] and references therein). Further, the lack of basalt and the presence of



Fig. 1. Simplified bathymetric map of Lena Trough and dredging locations. The Lena Trough axis is less than 80 km away from the continental margin. D88, D89, D90 refer to the sampling stations collected during cruise ARK XV/2 with PFS *Polarstern*.

strong seismic reflectors support a simple-shear model in which the subcontinental mantle was tectonically unroofed along large-scale detachment faults [12,13]. Serpentinite–sediment associations observed in the western and central Alps also indicate large-scale outcrops of serpentinites with rare basalt occurrences along the Tethyan continental margin in the Jurassic [14,15].

During a recent cruise with PFS *Polarstern*, we sampled basement highs along the Lena Trough axis for the first time and collected serpentinized peridotites, hydrothermal sulfides and glassy basalts [16]. Here we report major and trace element mineral data on plagioclase- and vein-free peridotites from this sample set in order to try to place constraints on their tectonic setting and melting history.

## 2. Geological setting

Lena Trough is a 300 km long linear deep located north of the coasts of Greenland and Spitsbergen in the Arctic Ocean, at minimal distance between North America and Eurasia (Fig. 1). It forms the connection between the amagmatic Molloy Ridge in the south and the orthogonally spreading and magmatically robust Gakkel Ridge in the north. An up to 500 m thick sediment pile covers its 3800–4400 m deep axial valley across most of its length [17]. Only a few north–south trending basement highs at the flanks of the axial deep remain sediment-free. At a few locations, the estimated axial basement depth reaches nearly 5000 m [17].

One important aspect of Lena Trough is its obliquity to the regional spreading direction. Normally, mid-ocean ridges spread in a direction that is perpendicular to the trend of the rift axis. However, in some cases the rift axis trends at a significant angle to the spreading direction. This can be determined by comparing the trend of the rift valley with the bearing to the spreading pole of the two plates involved. Oblique spreading reduces the effective spreading rate by making the same amount of mantle upwell along a longer section of ridge than in the orthogonal case.

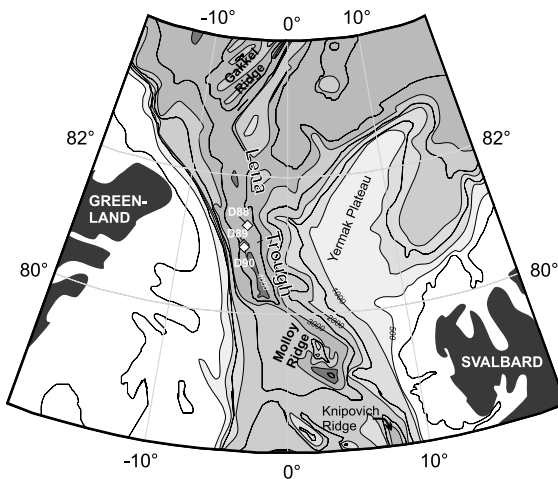The azimuth to the spreading pole between the

North American and Eurasian plates is approximately 034° here, and the axis of Lena Trough trends 349°, implying a spreading obliquity of about 55°. Given the slowness of the spreading rate ($\sim$13 mm/yr full rate) and this apparent obliquity, an effective full spreading rate of 7.5 mm/yr can be calculated. This is significantly slower than any other mid-ocean ridge that has ever been surveyed. Thus we expect that the effective spreading rate will have a significant effect on any melting that occurs there.

It is not at all clear what type of magmatic construction might occur at an effective full spreading rate of 7.5 mm/yr, if any. At the ultra-slow-spreading Gakkel Ridge, a variety of spreading morphologies are present in a completely orthogonal ridge where the full spreading rate varies between 13 and 10 mm/yr [18]. Lena Trough appears to have a rift morphology similar to that of the sparsely magmatic central portion of Gakkel Ridge, or the Oblique Spreading Center on the SW Indian Ridge near 12°E [9]. This involves a deep rift valley that does not stairstep (i.e. segmentation is not controlled by fracture zones), and where faults are parallel to the trend of the ridge (and not perpendicular to the spreading direction).

Another factor to consider is the proximity of Lena Trough to the Spitsbergen and Greenland continental margins. One possible effect of this proximity could be that Lena Trough is a sparsely magmatic rifted margin, where almost no partial melting has taken place. Whatever chemical signatures are recorded in exposed mantle rocks, they could be inherited from ancient melting events that long predate the recent rifting event. Such age relationships are seen at Zabargad Island, in the Red Sea Rift [19,20], and in the Ligurian ophiolites [21]. Another and less extreme possibility is that the proximity of the continental land masses on either side has contributed to cooling of the lithosphere and suppressing melt formation. This would be an extreme example of the 'lithospheric cap' effect thought to be responsible for the drop in crustal thickness with spreading rate [22].

Table 1
Sampling locations and modal composition of Lena Trough peridotites

| Sample # | Lithology | Estimated primary modes | | | |
|---|---|---|---|---|---|
| | | Ol | Opx | Cpx | Sp |
| PS55-D89: 80°58.0′N, 2°37.0′W; WD 3640–2960 m | | | | | |
| 89-7 | lherzolite | 70 | 23 | 6 | 1 |
| 89-9 | harzburgite | 78 | 19 | 3 | 1 |
| 89-11 | lherzolite | 68 | 25 | 6 | 1 |
| 89-13 | lherzolite | 70 | 20 | 9 | 1 |
| 89-14 | harzburgite | 65 | 30 | 4 | 1 |
| 89-17 | mylon. peridotite | | | | |
| 89-21 | harzburgite | 84 | 13 | < 1 | 2 |
| 89-24 | lherzolite | 74 | 20 | 5 | 1 |
| 89-25 | harzburgite | 70 | 25 | 4 | 1 |
| 89-27 | harzburgite | 71 | 25 | 3 | 1 |
| 89-28 | lherzolite | 64 | 25 | 10 | 1 |
| 89-30 | harzburgite | 70 | 26 | 3 | 1 |
| PS55-D90: 80°54.5′N, 2°27.4′W; WD 3950–3500 m | | | | | |
| 90-14 | mylon. peridotite | | | | |
| 90-19 | mylon. peridotite | | | | |
| 90-20 | harzburgite | 83 | total px: 16 | | 1 |
| 90-21 | serp. breccia | | | | |
| 90-23 | mylon. peridotite | | | | |
| 90-25 | harzburgite | 82 | total px: 17 | | 1 |

## 3. Results

### 3.1. Sampling and petrography

Basement rocks were recovered along the steep walls of the axial valley by dredging during the *Polarstern* ARK XV/2 cruise in 1999 [16]. The sampling locations are shown in Fig. 1. Massive sulfides and hydrothermal sediments and blue clayey serpentinite chunks were collected in dredge haul PS55-088, suggesting that these hydrothermal ore deposits are peridotite-hosted. Dredge hauls PS55-89 and 90 contained 78 and 3 kg of serpentinized peridotites, respectively. The latter also yielded 200 kg of highly vesicular pillow basalts with fresh glass. The detailed petrology and geochemistry of these olivine–phyric alkali basalts ($Na_2O$ 3.9 wt%; $K_2O$ 1.6 wt%; Mg# 0.62) will be reported elsewhere [23]. These lithologies are similar to those collected at mature slow-spreading mid-ocean ridges.

Twenty-four peridotite samples from these dredging stations were studied by electron and ion microprobe (Table 1). All serpentinized peridotites are optically devoid of plagioclase or cross-cutting magmatic veins. Primary modes

were reconstructed by point-counting normal rectangular thin sections in a $200 \times 200$ µm grid. The degree of serpentinization is generally larger than 90%. In some samples the high degree of serpentinization does not allow a clear optical distinction between former clinopyroxene (cpx) and orthopyroxene (opx). Serpentine pseudomorphs after pyroxene, however, can always be distinguished from the typical serpentine mesh structure after olivine. In such cases, only the total pyroxene content is listed (Table 1). The serpentinized mantle rocks have mainly coarse porphyroclastic textures except for three (ultra-)mylonitic samples (89-17, 89-18 and 89-23).

Also included in this study is a carbonate-cemented matrix-supported breccia (90-21), which contains angular serpentinite clasts of a few µm up to several cm. One of the larger serpentinite fragments in this sample contains well-preserved opx, cpx and spinel. Below, this coherent 'subsample' will be referred to as 90-21A. Furthermore, abundant angular Cr-spinel fragments (< 20–100 µm) are homogeneously distributed in the breccia. Judging from their colors in transmitted light (pale yellow to dark reddish brown), these peridotite-derived spinels do not have uni-

Table 2
Spinel major element compositions (in wt%) of Lena Trough peridotites

| Sample | Group | $n$ | $TiO_2$ | $Al_2O_3$ | $Cr_2O_3$ | FeO t | MgO | MnO | NiO | Total | Mg# (2+) | Cr# |
|--------|-------|-----|---------|-----------|-----------|-------|------|------|------|---------|----------|------|
| 89-7   | N | 6  | 0.05 | 53.71 | 14.16 | 12.76 | 19.36 | 0.13 | 0.33 | 100.50 | 0.76 | 0.150 (4) |
| 89-9   | F | 7  | 0.04 | 51.30 | 17.53 | 12.00 | 19.27 | 0.14 | 0.32 | 100.58 | 0.76 | 0.186 (4) |
| 89-11  | N | 6  | 0.03 | 54.89 | 13.36 | 11.86 | 19.82 | 0.12 | 0.34 | 100.42 | 0.78 | 0.140 (11) |
| 89-13  | N | 10 | 0.03 | 54.48 | 13.44 | 12.35 | 19.56 | 0.13 | 0.31 | 100.30 | 0.77 | 0.142 (22) |
| 89-14  | N | 8  | 0.04 | 53.69 | 14.35 | 12.61 | 19.40 | 0.12 | 0.33 | 100.53 | 0.76 | 0.152 (21) |
| 89-17  | N | 5  | 0.07 | 37.41 | 29.90 | 17.13 | 15.44 | 0.20 | 0.17 | 100.32 | 0.66 | 0.349 (8) |
| 89-21  | F | 8  | 0.07 | 25.11 | 44.12 | 17.25 | 13.75 | 0.28 | 0.09 | 100.66 | 0.62 | 0.541 (16) |
| 89-24  | N | 4  | 0.03 | 53.03 | 14.91 | 12.50 | 19.44 | 0.13 | 0.32 | 100.37 | 0.77 | 0.159 (8) |
| 89-25  | N | 10 | 0.04 | 53.99 | 14.67 | 11.20 | 20.06 | 0.12 | 0.34 | 100.43 | 0.79 | 0.154 (11) |
| 89-27  | N | 6  | 0.02 | 55.08 | 13.79 | 12.25 | 20.07 | 0.15 | 0.34 | 101.71 | 0.78 | 0.144 (8) |
| 89-28  | N | 4  | 0.02 | 53.70 | 14.52 | 12.63 | 19.37 | 0.13 | 0.32 | 100.69 | 0.76 | 0.154 (4) |
| 89-30  | N | 7  | 0.11 | 34.89 | 32.85 | 17.01 | 15.61 | 0.23 | 0.15 | 100.85 | 0.67 | 0.387 (12) |
| 90-14  | – | 9  | 0.04 | 53.79 | 14.18 | 12.91 | 19.28 | 0.15 | 0.30 | 100.66 | 0.76 | 0.150 (5) |
| 90-19  | – | 2  | 0.21 | 38.63 | 29.49 | 16.56 | 15.60 | 0.16 | 0.15 | 100.79 | 0.65 | 0.339 (–) |
| 90-20  | H | 8  | 0.10 | 37.41 | 30.84 | 16.03 | 15.85 | 0.22 | 0.13 | 100.57 | 0.67 | 0.356 (11) |
| 90-21A | H | 4  | 0.16 | 39.65 | 29.35 | 13.16 | 16.66 | 0.22 | 0.18 | 99.38  | 0.69 | 0.332 (11) |
| 90-23  | – | 8  | 0.04 | 51.38 | 16.73 | 12.64 | 18.90 | 0.14 | 0.27 | 100.10 | 0.76 | 0.179 (10) |
| 90-25  | H | 9  | 0.21 | 33.00 | 35.80 | 16.70 | 15.16 | 0.24 | 0.11 | 101.22 | 0.65 | 0.421 (7) |

Grouping based on REE patterns (N, normal; F, flat; H, hump-shaped). FeO t denotes total iron as FeO; Mg# (2+) using only ferrous iron calculated after [64]. Number in parentheses denotes one standard deviation.

form compositions. All spinel clasts are fresh and show no sign of alteration.

## 3.2. Mineral compositions

Relict primary phases (pyroxenes and spinel) were analyzed for major elements on a five-spectrometer Jeol JXA 8900RL electron probe microanalyzer at the University of Mainz. Spinels were measured using an acceleration potential of 20 kV, a beam current of 20 nA and a spot size of 2 μm. For cpx and opx, these conditions were reduced to 15 kV and 12 nA.

Cpxs were analyzed for trace elements (selected rare earth elements (REE) and Ti, V, Cr, Sr, Y, Zr; Table 4) by secondary ion mass spectrometry on a recently upgraded Cameca IMS-3f at the Max-Planck-Institut für Chemie in Mainz. Spots were selected for ion probe analysis after detailed petrographic and electron microprobe study. Only optically clear domains that show no signs of alteration or opx exsolution were analyzed. A primary beam current of 10 nA and a spot size of $\sim$10–15 μm were used, applying an energy offset of $-80$ V to filter for molecular interferences. Detailed analytical conditions are reported in [24]. For a single analysis, the overall accuracy, based on the long-term reproducibility of a low-concentration standard GOR132-G [25], is better than 20% for all REE and better than 12% for all other trace elements (95% confidence level).

### 3.2.1. Spinel

Spinel major element compositions could be determined for 18 samples (Table 2). Peridotites in both dredge hauls display a very large variation in average spinel Cr# [= molar Cr/(Cr+Al) ratio], which covers almost the entire spectrum of plagioclase-free abyssal peridotites. Most samples are relatively fertile with Cr# between 0.14 and 0.16. Significant within-sample variation (standard deviation on Cr# > $\sim$0.02) was observed for three samples (89-13, 89-14, 89-21). All other samples were compositionally homogeneous on a thin section scale. The low Ti concentration in the spinels of dredge 89 peridotites attests to the residual (plagioclase-free) nature of these samples (Fig. 2a), since spinels of plagioclase-bearing peridotite

generally have elevated Ti contents [26]. Spinels in two samples of dredge 90 have slightly elevated Ti concentrations ($\sim$0.2 wt% TiO$_2$). More than 100 individual spinel compositions were determined on two rectangular thin sections of the breccia sample 90-21. In terms of Cr#, the spinel fragments in the breccia display a bimodal distribution, with a broad maximum around 0.37 and a more narrow maximum around 0.19 ($n = 104$). These maxima coincide with the values of the coherent peridotite samples of both dredges (Fig. 2b). However, dredge 89 has significantly more fertile samples with much lower spinel Cr# than dredge 90. Many of the Cr-rich spinel fragments also have elevated Ti concentrations (Fig. 2a).
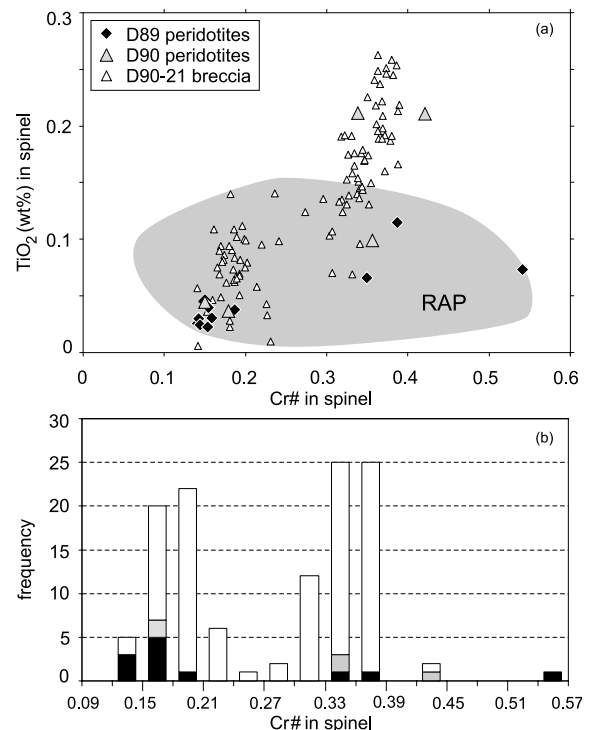


Fig. 2. (a) Cr# (= molar Cr/([Cr+Al]) vs. TiO$_2$ (wt%) in spinels from Lena Trough peridotites. Field for RAPs shown for comparison. RAP data [24,29,32,46,53,56] and unpublished results. (b) Spinel Cr# histogram showing bimodal distribution of spinel fragments in breccia 90-21 (white bars), in agreement with the compositions of the coherent peridotite samples of dredge 89 (black) and 90 (gray).

Table 3
Clinopyroxene major element compositions (in wt%) of Lena Trough peridotites

| Sample | Group | n | SiO2 | 1 S.D. | TiO2 | 1 S.D. | Al2O3 | 1 S.D. | Cr2O3 | 1 sd | FeO | 1 S.D. | MgO | 1 S.D. | MnO | 1 S.D. | CaO | 1 S.D. | NiO | 1 S.D. | Na2O | 1 S.D. | K2O | 1 S.D. | Total | Mg# |
|---|---|---|---|---|---|---|---|---|---|---|---|---|---|---|---|---|---|---|---|---|---|---|---|---|---|---|
| 89-7 | N | 8 | 51.92 | 0.26 | 0.20 | 0.04 | 6.43 | 0.28 | 1.19 | 0.07 | 2.63 | 0.31 | 15.50 | 0.94 | 0.09 | 0.04 | 21.38 | 1.12 | 0.04 | 0.03 | 1.12 | 0.08 | 0.00 | 0.01 | 100.50 | 0.913 |
| 89-9 | F | 4 | 52.71 | 0.38 | 0.15 | 0.03 | 4.91 | 0.04 | 0.97 | 0.03 | 2.33 | 0.18 | 16.57 | 0.59 | 0.10 | 0.01 | 22.14 | 0.76 | 0.05 | 0.03 | 0.61 | 0.06 | 0.01 | 0.01 | 100.54 | 0.927 |
| 89-11 | N | 9 | 52.55 | 0.33 | 0.23 | 0.03 | 5.70 | 0.48 | 1.02 | 0.13 | 2.58 | 0.21 | 15.85 | 0.77 | 0.10 | 0.03 | 21.49 | 0.88 | 0.05 | 0.03 | 1.11 | 0.09 | 0.01 | 0.01 | 100.68 | 0.916 |
| 89-13 | N | 14 | 51.91 | 0.26 | 0.19 | 0.04 | 6.40 | 0.35 | 1.17 | 0.09 | 2.61 | 0.19 | 15.45 | 0.53 | 0.11 | 0.03 | 21.57 | 0.66 | 0.05 | 0.02 | 1.10 | 0.06 | 0.00 | 0.00 | 100.56 | 0.913 |
| 89-14 | N | 15 | 52.38 | 0.34 | 0.21 | 0.05 | 5.77 | 0.50 | 1.02 | 0.12 | 2.56 | 0.19 | 15.89 | 0.67 | 0.09 | 0.03 | 21.46 | 0.64 | 0.05 | 0.02 | 1.08 | 0.09 | 0.01 | 0.01 | 100.52 | 0.917 |
| 89-17 | N | 2 | 51.86 | | 0.16 | | 3.02 | | 1.19 | | 2.32 | | 16.37 | | 0.06 | | 22.30 | | 0.04 | | 0.78 | | 0.02 | | 98.11 | 0.926 |
| 89-21 | F | 4 | 54.34 | 0.33 | 0.03 | 0.03 | 2.52 | 0.20 | 1.16 | 0.02 | 2.29 | 0.42 | 18.65 | 1.47 | 0.09 | 0.03 | 20.89 | 2.15 | 0.06 | 0.04 | 0.55 | 0.11 | 0.00 | 0.01 | 100.59 | 0.936 |
| 89-24 | N | 14 | 52.19 | 0.36 | 0.20 | 0.04 | 5.77 | 0.23 | 1.03 | 0.06 | 2.49 | 0.17 | 15.67 | 0.76 | 0.09 | 0.02 | 21.66 | 0.96 | 0.04 | 0.03 | 1.13 | 0.05 | 0.01 | 0.01 | 100.26 | 0.918 |
| 89-25 | N | 13 | 52.50 | 0.40 | 0.29 | 0.05 | 6.24 | 0.34 | 1.07 | 0.06 | 2.43 | 0.16 | 15.81 | 0.47 | 0.09 | 0.02 | 20.93 | 0.56 | 0.04 | 0.02 | 1.24 | 0.07 | 0.01 | 0.01 | 100.65 | 0.921 |
| 89-27 | N | 7 | 52.58 | 0.25 | 0.23 | 0.05 | 5.84 | 0.23 | 1.00 | 0.11 | 2.60 | 0.14 | 15.98 | 0.50 | 0.10 | 0.03 | 22.14 | 0.53 | 0.04 | 0.02 | 1.11 | 0.05 | 0.01 | 0.01 | 101.62 | 0.916 |
| 89-28 | N | 7 | 51.98 | 0.44 | 0.23 | 0.03 | 6.16 | 0.59 | 1.11 | 0.08 | 2.46 | 0.14 | 15.23 | 0.28 | 0.09 | 0.03 | 21.93 | 0.26 | 0.04 | 0.02 | 1.11 | 0.05 | 0.01 | 0.01 | 100.35 | 0.917 |
| 90-20 | H | 4 | 53.73 | 0.27 | 0.15 | 0.06 | 4.71 | 0.09 | 2.07 | 0.08 | 2.21 | 0.13 | 15.73 | 0.24 | 0.10 | 0.03 | 20.72 | 0.66 | 0.05 | 0.02 | 1.50 | 0.03 | 0.01 | 0.00 | 100.96 | 0.927 |
| 90-21A | H | 5 | 52.73 | 0.17 | 0.24 | 0.04 | 5.53 | 0.24 | 1.79 | 0.02 | 2.37 | 0.17 | 15.41 | 0.28 | 0.11 | 0.03 | 20.59 | 0.42 | 0.05 | 0.03 | 1.62 | 0.10 | 0.00 | 0.01 | 100.45 | 0.921 |
| 90-25 | H | 11 | 53.48 | 0.24 | 0.27 | 0.05 | 4.64 | 0.24 | 2.02 | 0.07 | 2.08 | 0.09 | 15.79 | 0.29 | 0.10 | 0.03 | 20.95 | 0.57 | 0.03 | 0.02 | 1.72 | 0.08 | 0.01 | 0.01 | 101.10 | 0.931 |

Grouping is based on REE patterns (N, normal; F, flat; H, hump-shaped). See text. 1 S.D. is one standard deviation.

### 3.2.2. Cpx

Major element compositions of cpx are listed in Table 3. Compared to abyssal peridotites, the Lena Trough samples are very sodium-rich (Na2O 0.55–1.72 wt%), even at high spinel Cr# (Fig. 3). The majority of the Lena Trough peridotites plot outside the compositional field of residual abyssal peridotites (RAPs) at low spinel Cr# and high Na2O. Other major element characteristics are similar to other abyssal peridotite cpx, with the exception of very high chromium contents (Cr2O3 ~ 2.05 wt%) in the two coherent
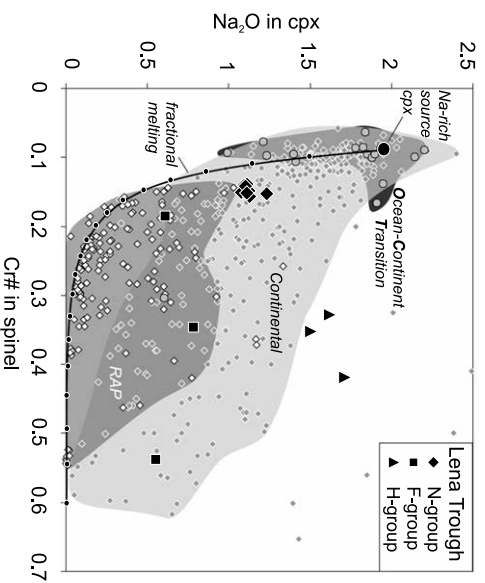


Fig. 3. Na2O content (wt%) in Lena Trough cpx vs. Cr# of associated spinels. Although there is a large overlap, the majority of RAPs (white diamonds) have a lower sodium content than continental peridotites at a given spinel Cr#, thought to result from a metasomatic overprint in the latter. OCT (gray circles) peridotites appear to be restricted to highly fertile low Cr#/high Na compositions, which overlap with the majority of continental peridotites (gray diamonds). Most Lena Trough peridotites have low Cr# associated with ocean and continental mantle. The grouping of Lena Trough samples is based on REE patterns (see text). Also shown is a fractional melting trajectory, illustrating that many RAP are not strictly residues of near-fractional spinel-field melting ($D_{Na}$ from [47]). Data continental: [57–61] and the major element mineral composition database of Smith (available at www.geo.utexas.edu) filtered for Grand Canyon xenoliths (D. Ionov, personal communication), TiO2 in spinel > 0.4 wt%, Mg# opx < 0.88 and > 5% deviations from linear Cr# spinel–cpx relationship. Data OCT: [7,62]. Data RAP: [24,29,32,46,53,56].

Table 4
Clinopyroxene trace element concentrations (in μg/g) of Lena Trough peridotites

| Sample | Group[a] | n | Ti | ±[b] | V | ± | Sr | ± | Y | ± | Zr | ± | La | ± | Ce | ± | Nd | ± | Sm | ± | Eu | ± | Gd | ± | Dy | ± | Er | ± | Yb | ± |
|---|---|---|---|---|---|---|---|---|---|---|---|---|---|---|---|---|---|---|---|---|---|---|---|---|---|---|---|---|---|---|
| 89-7 | N | 2 | 843 | 4 | 145 | 1 | 2.2 | 0.04 | 9.9 | 0.2 | 1.4 | 0.003 | 0.011 | 0.04 | 0.14 | 0.01 | 0.32 | 0.03 | 0.39 | 0.04 | 0.19 | 0.01 | 1.0 | 0.06 | 1.6 | 0.11 | 1.3 | 0.07 | 1.5 | 0.06 |
| 89-9 | F | 2 | 707 | 3 | 143 | 1 | 8.9 | 0.1 | 7.1 | 0.1 | 2.8 | 0.01 | 0.27 | 0.1 | 0.89 | 0.03 | 0.69 | 0.06 | 0.32 | 0.03 | 0.14 | 0.01 | 0.74 | 0.05 | 1.1 | 0.07 | 0.81 | 0.05 | 1.0 | 0.05 |
| 89-11 | N | 3 | 972 | 4 | 162 | 1 | 2.0 | 0.03 | 9.7 | 0.1 | 1.4 | 0.002 | 0.006 | 0.03 | 0.14 | 0.01 | 0.54 | 0.04 | 0.45 | 0.01 | 0.21 | 0.01 | 1.0 | 0.05 | 1.7 | 0.07 | 1.3 | 0.05 | 1.4 | 0.04 |
| 89-13 | N | 3 | 932 | 3 | 155 | 1 | 2.2 | 0.04 | 9.8 | 0.1 | 1.4 | 0.002 | 0.008 | 0.04 | 0.13 | 0.01 | 0.59 | 0.03 | 0.50 | 0.05 | 0.23 | 0.01 | 1.0 | 0.05 | 1.7 | 0.07 | 1.2 | 0.05 | 1.5 | 0.05 |
| 89-14 | N | 3 | 1057 | 6 | 174 | 1 | 2.1 | 0.04 | 9.4 | 0.1 | 1.5 | 0.002 | 0.008 | 0.04 | 0.13 | 0.01 | 0.53 | 0.04 | 0.48 | 0.05 | 0.18 | 0.01 | 0.9 | 0.06 | 1.5 | 0.06 | 1.1 | 0.04 | 1.2 | 0.04 |
| 89-17 | N | 2 | 708 | 10 | 142 | 2 | 6.8 | 0.1 | 2.7 | 0.1 | 3.0 | 0.005 | 0.037 | 0.08 | 0.32 | 0.02 | 0.54 | 0.04 | 0.27 | 0.04 | 0.10 | 0.01 | 0.3 | 0.04 | 0.5 | 0.04 | 0.4 | 0.04 | 0.4 | 0.03 |
| 89-21 | F | 3 | 190 | 1 | 117 | 1 | 27 | 1 | 1.3 | 0.05 | 2.9 | 0.01 | 0.23 | 0.03 | 0.46 | 0.01 | 0.60 | 0.03 | 0.26 | 0.01 | 0.11 | 0.01 | 0.35 | 0.02 | 0.31 | 0.02 | 0.16 | 0.01 | 0.23 | 0.01 |
| 89-24 | N | 2 | 1032 | 4 | 161 | 1 | 2.0 | 0.02 | 9.7 | 0.2 | 1.6 | 0.002 | 0.011 | 0.04 | 0.13 | 0.01 | 0.56 | 0.05 | 0.47 | 0.04 | 0.24 | 0.02 | 1.1 | 0.06 | 1.8 | 0.08 | 1.2 | 0.05 | 1.4 | 0.05 |
| 89-25 | N | 2 | 1594 | 7 | 159 | 2 | 5.6 | 0.1 | 10.3 | 0.2 | 5.8 | 0.003 | 0.021 | 0.1 | 0.47 | 0.02 | 1.4 | 0.07 | 0.90 | 0.05 | 0.37 | 0.02 | 1.5 | 0.07 | 2.0 | 0.09 | 1.3 | 0.06 | 1.3 | 0.05 |
| 89-28 | N | 2 | 1006 | 4 | 152 | 1 | 2.0 | 0.03 | 9.4 | 0.1 | 1.6 | 0.002 | 0.009 | 0.04 | 0.14 | 0.01 | 0.50 | 0.04 | 0.52 | 0.04 | 0.24 | 0.02 | 1.0 | 0.06 | 1.6 | 0.08 | 1.1 | 0.06 | 1.3 | 0.05 |
| 90-20 | H | 3 | 824 | 3 | 124 | 1 | 66 | 0.2 | 7.7 | 0.1 | 51 | 0.01 | 0.18 | 0.2 | 2.9 | 0.04 | 5.9 | 0.10 | 2.2 | 0.07 | 0.77 | 0.02 | 2.6 | 0.08 | 1.7 | 0.08 | 0.85 | 0.04 | 1.0 | 0.04 |
| 90-21A | H | 5 | 1236 | 3 | 129 | 1 | 3.0 | 0.03 | 8.2 | 0.1 | 4.1 | 0.001 | 0.008 | 0.04 | 0.15 | 0.01 | 0.81 | 0.03 | 0.68 | 0.03 | 0.41 | 0.04 | 1.2 | 0.06 | 1.5 | 0.06 | 1.0 | 0.03 | 1.2 | 0.03 |
| 90-25 | H | 3 | 1314 | 4 | 159 | 1 | 48 | 0.2 | 9.5 | 0.2 | 27 | 0.01 | 0.20 | 0.1 | 1.1 | 0.03 | 1.8 | 0.06 | 1.15 | 0.05 | 0.55 | 0.05 | 1.9 | 0.08 | 2.1 | 0.08 | 1.1 | 0.04 | 1.2 | 0.04 |
| GOR132-std G | | 15 | 1690 | 72[c] | 190 | 10 | 15 | 0.5 | 13.0 | 0.4 | 10.3 | 0.010 | 0.086 | 0.4 | 0.40 | 0.02 | 0.69 | 0.05 | 0.55 | 0.05 | 0.28 | 0.02 | 1.2 | 0.09 | 2.36 | 0.21 | 1.53 | 0.10 | 1.51 | 0.09 |

[a] Grouping based on REE patterns (N, normal; F, flat; H, hump-shaped).
[b] For all samples: weighted mean (internal) error.
[c] One standard deviation (external error).

peridotites from dredge 90. All cpx grains are homogeneous and significant within-sample variation has not been observed.

Based on their REE patterns, the Lena Trough peridotites can be divided into three groups: normal (N), flat (F) and hump-shaped (H). Nine out of 14 cpx-bearing samples are light (L-) REE-depleted and have flat middle (M-) to heavy (H-) REE patterns around six to nine times chondrite. This is typical of LREE-depleted RAPs [24,27–30] (Fig. 4a). In an extended REE diagram, the N-group samples are also characterized by negative Zr and Ti anomalies and no significant Sr anomaly (Fig. 4c). In terms of major element composition, the N-group samples have uniformly low spinel Cr# ($\sim$0.15), and intermediate sodium (1.1–1.3 wt% $Na_2O$) concentrations (Fig. 3).

Five samples have trace element signatures that are not typical of melting residues. Compared to the N-group REE patterns, the F-group samples 89-9 and 89-21 have almost flat REEs, nearly chondritic LREE concentrations, but different HREE contents ($\sim$five and one times chondritic, respectively). Furthermore, 89-21 has a significant positive Sr anomaly, which is absent in 89-9. Both samples have negative HFSE anomalies. Samples 90-20 and 90-25 have a hump-shaped REE pattern, which is well pronounced in the former (($Sm/Yb)_N$ = 2.7). A Zr anomaly is absent in both samples (Fig. 4d). Coarse cpxs intergrown with spinel clasts of the mylonitic peridotite 89-17 have a trace element pattern that is intermediate between the ultra-HREE depleted flat pattern of 89-21 and the normal patterns.

As shown in Fig. 5, all N-group peridotites lie on the well-established correlation between Cr# in spinel and HREE concentrations in associated cpx [31]. Only the samples with the hump-shaped REE patterns (90-20 and 90-25) plot off the melting trend. Such REE patterns can be explained by late-stage deep entrapment of LREE-depleted melt [24]. Remarkable is the good fit of the F-group samples. Despite their nearly flat REE patterns, the HREE Er and Yb appear not to be strongly affected by the process(es) that disturbed the correlation between major element melting indicators and the highly incompatible trace elements (e.g. the LREE).
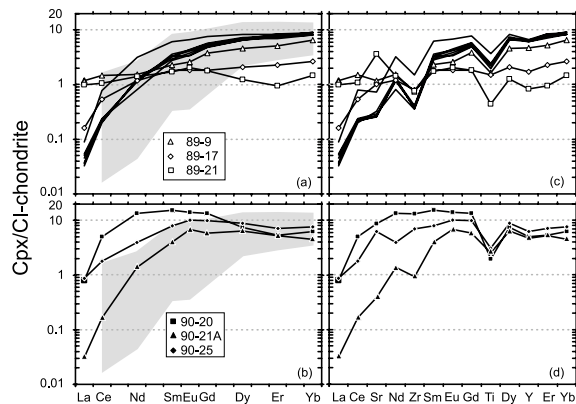
Fig. 4. Chondrite-normalized REE and trace element abundances in cpx from Lena Trough peridotites. Shown for comparison (gray field) are the Southwest Indian and American–Antarctic Ridge peridotite cpx data [27]. Most samples ($n = 9$, no symbols) in dredge 89 (panels a and c) are LREE-depleted normal melting residues denoted N-group in the text. Two unfractionated samples in this dredge haul have relatively flat REE patterns (F-group). Hump-shaped REE patterns (H-group) in dredge 90 peridotites (panels b and d) indicate late-stage melt entrapment. Chondrite values are from [63].

## 4. Discussion

### 4.1. Melting

#### 4.1.1. Degree of melting

It has been shown previously that spinel Cr# serves as a good qualitative indicator for the degree of melting that plagioclase-free and vein-free peridotitic residues have undergone [32]. Applying the good correlation between HREE concentrations in cpx and Cr# in associated spinels, this melting indicator can be used quantitatively to estimate the absolute degree of melting [31]. Based on this method, which assumes a DMM spinel lherzolite starting composition [27], the average degree of fractional (i.e. minimum) melting for the N-group peridotites is 5%. Melting models that account for a residual melt porosity would not yield significantly higher degrees of melting.

Dredge 90 contained peridotites with hump-shaped cpx REE patterns that plot off the correlation between Cr# in spinel and HREE in cpx (Fig. 5). Hump-shaped patterns are not residues of garnet melting [27], but instead are consistent

with melt refertilization [24]. The dredge 90 samples, similar to some other samples with hump-shaped REE patterns, lie slightly above the HREE–Cr# trend, suggesting that the HREE can be affected during this process. In any event, the degree of melting cannot be estimated from the spinel Cr# in samples with hump-shaped REE patterns.

#### 4.1.2. The effect of garnet in the melting residue

The N-group peridotites in dredge 89 are characterized by fractionated M-HREE ratios at relatively high HREE concentrations, which cannot be explained by fractional melting in the stability field of spinel peridotite (Fig. 6). Such fractionations can be generated by initial melting of a garnet peridotite followed by spinel-facies reequilibration and subsequent melting of spinel peridotite [24]. Fig. 6 shows the results of such a polybaric fractional melting model. Both melting trajectories for cpx in equilibrium with residual garnet, and spinel-facies-projected cpx compositions are displayed. The projection simulates cessation of melting under garnet-facies conditions, followed by an instantaneous breakdown reaction from a garnet to a spinel peridotite assemblage. It presents the equilibrium cpx composition after ascent into the spinel peridotite stability field. A
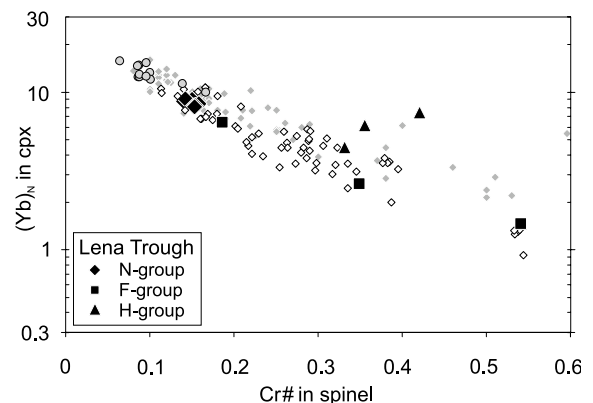


Fig. 5. Cr# in spinels vs. chondrite-normalized Yb concentration in associated cpx of continental peridotite xenoliths (gray diamonds), RAPs (open diamonds), plagioclase-free OCT peridotites (gray circles) and Lena Trough peridotites (closed symbols). The hump-shaped peridotites of dredge 90 plot off the correlation, supporting a non-residual origin. Data sources in the caption of Fig. 3.

detailed explanation of this calculation is given by [24].

The fractionated Sm/Yb ratios and high Yb concentrations of the N-group peridotites can be explained by 4–6% melting in the stability field of garnet peridotite, followed by another 3–4% under spinel-facies conditions. This value deviates strongly from the degree of melting obtained on the spinel compositions. The reason for this is most likely that melting in the stability field of garnet peridotite will not fractionate Cr from Al as strongly as melting with residual spinel. After ascent and melting under spinel-facies conditions this leads to an underestimation of the true degree of melting using the spinel Cr#.

This is particularly important for the Lena Trough samples, because roughly half of the total melt extraction occurred in the garnet–peridotite stability field. Compared to other abyssal peridotites, these samples have undergone the highest extent of garnet-field melting relative to the total amount of melt extraction. On the one hand, the garnet-field signatures suggest that the onset of melting occurred at depths exceeding ∼80 km, which implies a relatively high mantle potential
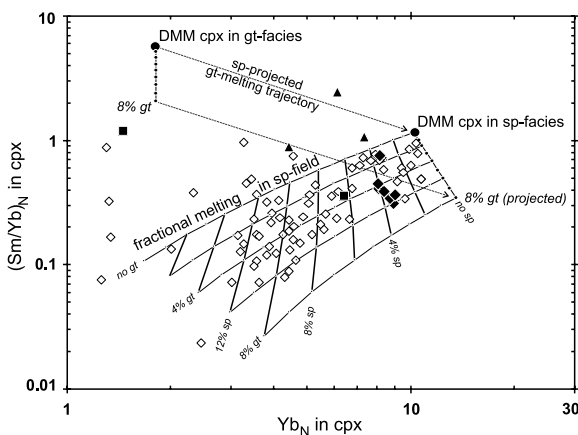


Fig. 6. Chondrite-normalized Yb vs. Sm/Yb in cpx. Also shown are results of fractional melting models of spinel and garnet peridotite sources, as well as garnet-facies melting followed by spinel-facies melting. N-group Lena Trough peridotites have strongly fractionated Sm/Yb ratios at relatively high Yb concentrations, which requires 4–6% garnet-field melting followed by another 3–4% spinel-field melting. This suggests deep onset, as well as deep cessation of melting. Symbols and data sources as in Fig. 5.

temperature [33–35], or a significant water content which would lower the solidus temperature [36]. On the other hand, the relatively limited spinel-facies melting suggests that the final depth of melting is deep compared to faster-spreading mid-ocean ridge settings.

These results are consistent with the tectonic setting of Lena Trough on a slow-spreading, highly oblique ridge near to a continental margin. Here, the lithosphere is probably thicker than at faster-spreading mid-ocean ridges. Such a thick conductively cooled lithospheric cap will lead to cessation of melting at depths that significantly exceed those of faster-spreading mid-ocean ridge settings. This may be the direct consequence of the extreme obliquity of the Lena spreading center and the resulting low effective spreading rate of ∼7.5 mm/yr, as well as the immediate vicinity to colder subcontinental lithosphere.

Deep melting in the presence of residual garnet is further supported by high La and low Yb content (10 and 1.8 ppm, respectively) of the dredge 90 alkali basalts [23]. Considering the different ascent velocities of melt and associated residue, deep melting underneath Lena Trough could have been occurring for one or possibly several million years. In a transform-parallel transect in the Vema Fracture Zone (equatorial Atlantic), systematic variations in the chemical compositions of basalts and residual peridotites were found [37]. Melting indicators in both basalts and peridotites display similar oscillatory variations, but the basalts appear to have been erupted 1.3 Myr before the associated peridotites reached the seafloor. In the case of Lena Trough, this would mean that the basalts that are associated with the studied peridotites should now be located off-axis.

## 4.2. Chemical variability

Because of the lack of spatial relationships beyond the size of a single sample, dredged peridotites are not ideally suited to address the scale, extent and causes of heterogeneities in residual mantle. Nevertheless, significant chemical variations in plagioclase-free and vein-free peridotites are present in some mid-ocean ridge dredge hauls

and absent in others [24]. The two ODP drill holes with significant penetration into residual mantle lithologies (Leg 147, Hess Deep and Leg 153, MARK area) are homogeneous almost to the level of analytical precision across several hundred meters of core [29,30]. The only exception to this is in the vicinity of late-stage magmatic veins [38].

The Lena Trough peridotites show nearly the entire variation in Cr# seen in ocean floor peridotites in just two dredge hauls. While adequate statistics have not as yet been compiled to address quantitatively whether this variation is more than on other mid-ocean ridges, qualitatively this appears so. The N-group Lena Trough peridotites have low spinel Cr# and normal LREE-depleted trace element patterns as is common for relatively fertile RAPs. As a group, they do not show large compositional variation. The non-residual samples (flat and hump-shaped REE patterns), which have clearly undergone some interaction with a percolating melt, have higher spinel Cr# and thus largely control the magnitude of local chemical variation. Spinel Cr# in dunite channels in the mantle section of ophiolites are generally higher than in the surrounding peridotites [39]. Their cpxs cover a large range from ultra-depleted to MORB-type compositions [39,40]. Similarly large chemical variations on an outcrop- to sub-km scale have not been observed in plagioclase- and vein-free peridotites from mid-ocean ridges and associated fracture zones. Arguably however, the abyssal peridotite data used for comparison are biased, because commonly less than five plagioclase-free samples per dredge haul are studied and considered to be representative.

The bimodal spinel Cr# distribution of the breccia 90-21 provides further constraints on the relative abundance of residual to non-residual mantle rocks at the dredge 90 outcrop. The low-Cr# peak, which is relatively tight, represents roughly a third of the total number of spinels in the breccia. It coincides with the Cr# of the LREE-depleted N-group samples, suggesting that the chemical signature of roughly a third of the dredge 90 slope/outcrop is dominated by near-fractional melt extraction. The high-Cr# peak with spinel Cr# around 0.35 is broader and coincides with the samples that have hump-shaped

REE patterns. It is likely that these non-residual peridotites were formed by a reaction of an N-group-type wall rock with an exotic melt. In order to generate the clear bimodal spinel Cr# distribution, melt transport must have been focused rather than diffuse. Without spatial information between the individual dredge 90 samples, it is unclear whether there are two separate units or a number of small-scale interfingering different melt transport channels. At dredge 89, which is located $\sim$ 6.5 km north of dredge 90, the N-group peridotites dominate, and non-residual peridotites play a subordinate role. These non-residual dredge 89 samples can obviously not be related to a possible dredge 90 melt transport channel. Alternatively, the bimodal distribution might be sampling two distinct units separated by a fault.

### 4.3. Refertilization and the sodium problem

Sodium is one of the key elements for the understanding of melting under mid-ocean ridges. Systematic global variations of sodium content in MORB glasses, if corrected for low-pressure fractional crystallization, have been used to estimate degrees of melting, variations in mantle potential temperature and crustal thickness [34,41]. In contrast, the behavior of sodium in melting residues is not well understood at all, as pointed out by a number of studies [42–44]. Many plagioclase-free abyssal peridotite cpxs exhibit higher sodium than would be predicted by isobaric fractional or low residual porosity melting. This is illustrated in Fig. 3, where the $Na_2O$ content of cpx is plotted as a function of the Cr# in the coexisting spinel. Most RAPs plot on or just above the fractional melting curve, but a significant fraction falls above significantly.

### 4.3.1. Analytical artifacts

Analytical artifacts have been claimed to be the cause of high sodium contents in some cpxs. A large fraction of the published abyssal peridotite cpx compositions was determined on fused, hand-picked grains [45,46]. Both Baker and Beckett [44] and Asimow [43] refer to a personal communication with H. Dick, who stated that this procedure could have led to elevated sodium concentrations.

However, recent in situ analyses of a number of the same samples that were previously studied by [45] have shown no significant discrepancies in the sodium contents of cpx [24], indicating that the sodium problem is not an analytical artifact. The very substantial Na enrichment in the Lena samples is far beyond what is explainable as an analytical artifact in any event.

### 4.3.2. No Na–LREE fractionation during partial melting

The cpx–melt distribution coefficient ($D^{cpx/l}$) of Na is very similar to that of Nd, with values around 0.2 [42,47,48]. As shown in Fig. 7a, a fractional melting trajectory of a DMM source nearly forms a straight line. In this Na–Nd diagram, many abyssal peridotites (the Lena Trough samples in particular) plot towards the Na-rich side of the melting trajectory, even if a sodium-rich mantle is used as a source. This suggests that sodium is less incompatible than Nd.

Recent partitioning experiments have shown that $D^{cpx/l}$ of Na is pressure-dependent, and decreases from ∼0.5, where melting may start around 3 GPa, to values less than 0.2 at the top of the melting column [48]. It therefore seems that sodium-rich, Nd-poor cpxs can be residues of high-pressure partial melting, and the sodium-poor cpxs are dominated by low-pressure melt extraction. Fig. 7a shows the results of a melting model in which extreme partition coefficients are used to obtain maximum fractionation ($D^{cpx/l}$ of Na and Nd are constant at values of 0.5 and 0.2, respectively). Although this model could explain some of the observed Na–Nd fractionation, the N-group Lena Trough cpxs still plot to the sodium-rich side of a melting curve.

The extreme $D^{cpx/l}$ for Na and Nd discussed above are probably unrealistic, and are shown to illustrate the maximum fractionation that can be obtained during partial melting. The reason for this is that $D^{cpx/l}$ of the REE are not constant either, but instead become less incompatible as a function of the sodium content of cpx [49]. Therefore, less incompatible $D$s for Nd would reduce the curvature of the melting trajectory. Furthermore, such $D$s for REE in cpx cannot generate the required fractionation of middle from the

heavy REE at high HREE concentrations [24]. As discussed in Section 4.1, this is the main evidence for initial melt extraction under garnet-facies conditions. Particularly the Lena Trough cpxs show this residual garnet signature, which is not in agreement with the high sodium concentrations. This strongly suggests that the origin for the high sodium concentration is not related to partial melting.

### 4.3.3. No Na-LREE fractionation during melt refertilization

Refertilization of depleted mantle peridotite by a basaltic melt is an explanation proposed for the sodium problem [42]. We modeled an Elthon-type refertilization (i.e. melt entrapment after melting and re-equilibration) for both sodium and the REE concentrations in cpx. Such a post-melting refertilization has been proposed to explain elevated sodium concentrations in cpx [42] and hump-shaped REE patterns in cpx [24]. This model simulates entrapment of small amounts of melt (melt–residue mixing), followed by crystallization and equilibrium trace element redistribution as a function of the mineral/liquid partition coefficients [24]. By varying the input parameters (initial whole-rock composition and mineral modes, composition of the infiltrating melt and crystallization mode), we tried to match both the REE pattern of the cpx and its sodium content, concentrating on the N-group Lena Trough peridotites. The results of these models are shown in Fig. 7b,c.

First we tested if any of the N-group Lena Trough peridotites could have been affected by a LREE-enriched melt, such as the alkali basalts collected in dredge 90. The starting mode was a lherzolite with 7% modal cpx. In terms of its trace element composition, we used the calculated residue of 6% fractional melting in the garnet peridotite stability field, followed by 4% melt extraction under spinel-facies conditions. As described in the previous section, the resulting REE pattern matches the M- to HREE of the N-group samples (Fig. 6). Fig. 7b,c shows refertilization calculations for two extreme crystallization modes ($Z_{ol}/Z_{cpx} = 0.9/0.1$ and $0.1/0.9$, respectively). The crystallization mode $Z$ does not influence the shape of
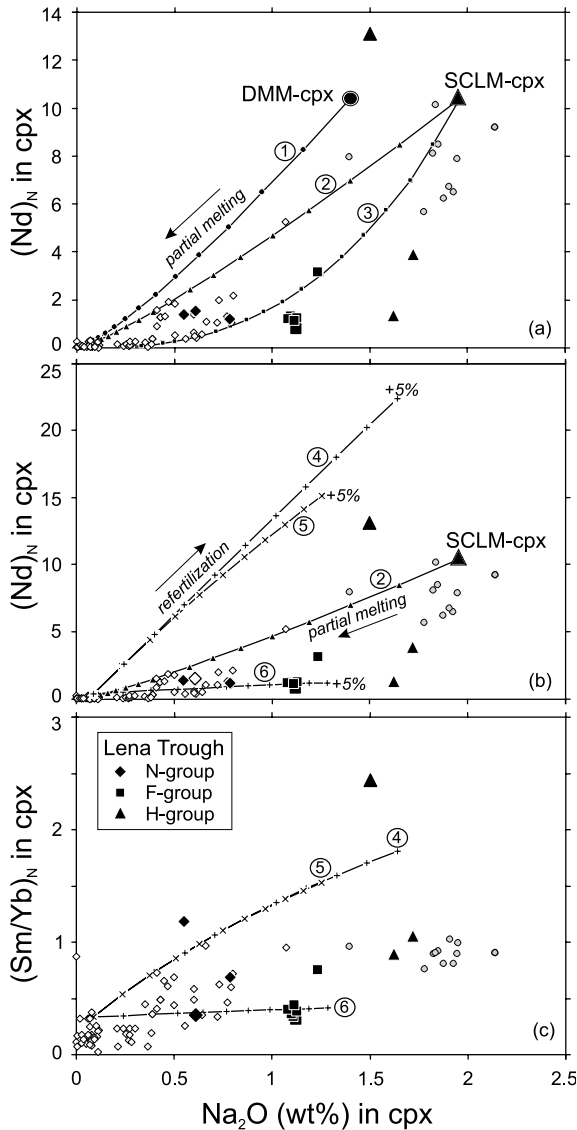
Fig. 7. (a,b) $Na_2O$ in cpx vs. chondrite-normalized Nd, and (c) Sm/Yb in cpx of Lena Trough and other abyssal peridotites. (1) Fractional melting of a depleted mantle source; (2) critical melting with 1% residual melt porosity and a Na-rich subcontinental lithospheric source; (3) same as (2) but with $D^{cpx/l}$ Na of 0.5. For all melting models 1% melting increment tick marks. (4,5) Refertilization models (0.5% melt addition increments) of a LREE-depleted lherzolite by a LREE-enriched alkali melt using ol/cpx crystallization modes of 0.9/0.1 and 0.1/0.9, respectively. Garnet-field melting signature is obscured by rapidly increasing Sm/Yb. (6) Refertilization by a Na-rich, REE-poor 'melt' can explain Lena Trough data, but such a melt composition is unrealistic. Symbols as in Fig. 5. See text for detailed discussion.

the trace element pattern, solely the absolute cpx trace element abundance. Entrapment and crystallization of a LREE-enriched, Na-rich melt will lead to a rapid increase of both Nd and Na in the equilibrated peridotite cpx (Fig. 7b). These curves are steeper than the melting curves, implying that refertilization with a LREE-rich, Na-rich melting cannot generate a LREE-depleted, Na-rich peridotite. Furthermore, small amounts of melt entrapment would lead to an increase of Sm/Yb, which would obscure the garnet field melting signature of the N-group peridotites (Fig. 7c).

A hypothetical melt that could produce the Lena cpx compositions requires high sodium contents ($\sim 4\%$ $Na_2O$), combined with extremely low ($< \sim 3\times$ chondritic) REE concentrations. Such a REE-poor melt would not affect Sm/Yb values and obscure a garnet-field signature. However, neither has such a melt been observed anywhere, nor do any peridotite melting models predict such liquids. Therefore, a classical refertilization of peridotite with a silicate melt cannot generate the required extreme fractionation between sodium and the L-MREE.

### 4.3.4. Refertilization by metasomatism or diffusive fractionation

The calculations above have demonstrated that sodium should behave like a similarly incompatible REE during partial melting and silicate melt refertilization. Therefore, sodium has to be fractionated from the LREE, possibly by a fluid in which sodium is more soluble than REE. Pervasive percolation of a hydrous fluid under subsolidus conditions might alter the mineral compositions of these residues, without necessarily leading to formation of hydrous phases such as amphibole or phlogopite. This type of metasomatism is common in mantle xenoliths from the subcontinental lithospheric mantle, but is believed to be absent in abyssal peridotites. However, in an OCT zone, such as the Lena Trough, elevated sodium concentrations might be inherited from subcontinental metasomatism, which allows us to shift the starting composition of the melting model to sodium values higher than DMM estimates (Fig. 7a). As discussed in Section 4.1, the degree of

melting has to be 10% in order to match the REE depletion of the cpx. The sodium concentration of the N-group samples is still much higher than the values calculated by melting a sodium-rich source. Thus, recent melting of a metasomatically modified (formerly subcontinental) mantle during the opening of Lena Trough cannot explain the high sodium contents either.

Finally, it is possible that Na is diffusively fractionated from other elements, either within an infiltrating melt [50], or in a solid state [51], or possibly, by a combination of both. Lundstrom's experiments [50] suggest that a melt that infiltrates wall-rock peridotite near a melt transport channel could have significantly higher Na/REE than the original melt, as a result of the high melt diffusivity of sodium. Such a diffusively fractionated melt that has obtained 'unrealistically' high Na/Nd values might have become entrapped within the sampled N-group peridotite. Although a diffusive fractionation could be responsible for the observed sodium enrichment in the Lena Trough and other abyssal peridotites, the lack of chemical gradients within and between samples does not allow rigorous testing. Furthermore, in order to maintain mass balance, in which Na is originally not fractionated from the LREE, Na enrichment has to be a local effect, counterbalanced by a relative Na depletion elsewhere. It is therefore very unlikely to obtain a widespread Na enrichment by diffusive fractionation within a percolating melt following the Lundstrom hypothesis [50].

The results from the models presented above provide a relative timeframe. First, near-fractional melting generated LREE- and Na-depleted residues. Then, sodium was re-enriched by metasomatism, although at this stage we can only speculate about its physical mechanism.

### 4.4. Near-margin tectonic setting

Partial melting beneath mid-ocean ridges, and thus crustal formation, are thought to be governed by a series of geodynamic 'forcing functions' that can in principle be linked to measurable geophysical quantities such as spreading rate, ridge obliquity, upwelling mantle temperature, and mantle compositional heterogeneity. At Lena

Trough, the combination of ultra-slow spreading and extreme obliquity are complicated by a third factor, the presence nearby of continental lithosphere. As is clear from Fig. 1, the distance from Lena Trough to the Greenland continental margin and the Yermak Plateau (1000 m isobath) is only 80 and 90 km, respectively.

### 4.4.1. Depression of the conductive geotherm

It is possible that the proximity to this continental margin serves to further depress the thermal regime beneath the ridge. This would explain certain qualitative aspects of the data sets, such as the apparently high potential temperature required to produce melting in the garnet field contrasted to limited melting in the spinel field. This would also help explain the apparently sudden transition from magmatically robust seafloor spreading in the western end of Gakkel Ridge [18] to amagmatic or sparsely magmatic crustal generation in Lena Trough.

However, it implies that the deep melting underneath Lena Trough was followed by a cryptic metasomatic event that led to the elevated sodium concentrations discussed in the previous section. If pervasive sodic metasomatism can occur under oceanic conditions at Lena Trough, then a similar process could be responsible for the generation of other sodium-rich abyssal peridotites [24,45,46,52,53].

### 4.4.2. Inherited melting/metasomatic signature

An alternative hypothesis is that the Lena Trough peridotites belong entirely to the subcontinental lithospheric mantle and are part of a nearly amagmatic rifted margin couple between Greenland and Spitsbergen. This supposition is not so far-fetched, as the distances involved are comparable to the width of the amagmatic portion of the Iberia Margin. It implies that the observed variation is not caused by the spreading-related decompression melting and reactive melt migration, but is inherited from the exhumed subcontinental lithosphere. The LREE depletion could be inherited from an earlier melt extraction event. The sodium enrichment would then result from metasomatism, after accretion to the subcontinental lithosphere.

This hypothesis is supported by isotopic studies on mantle rocks from other OCTs. The only known present-day active OCT is in the Red Sea. In this region between Africa and Arabia, rift-related mantle rocks are only known from Zabargad Island. Based on major element mineral compositions, the exposed peridotites are thought to represent the chemical transition from a subcontinental mantle to a suboceanic mantle (Fig. 3) [54]. However, osmium isotopic studies have shown that the depletion recorded by this peridotite body may have occurred in the Proterozoic [20]. This suggests that the chemical signature of the mantle phases was not necessarily generated during the opening of the Red Sea and that Zabargad may be an exhumed piece of subcontinental mantle [20]. In the Ligurian ophiolites [21], volcanics bearing a distinctly mid-ocean ridge signature erupt in conjunction with mantle with a much older melting history.

The principle that abyssal peridotites are to first order the complementary residues of MORB remains unchallenged, despite the scarcity of isotopic data [52,55]. It is not possible that abyssal peridotites in general represent fragments of an old passively exhumed mantle that inherited its chemical signature from an ancient ($> \sim 100$ Myr) melt extraction event without 'zero-age' melting. In such a case, their $^{143}Nd/^{144}Nd$ would be extremely high, resulting from their highly fractionated Sm/Nd ratios and the related rapid ingrowth of radiogenic Nd. Their Nd isotopic composition can only be explained by recent partial melting of a MORB-type mantle underneath the ridge. Some of these Southwest Indian Ridge peridotites, which have DMM-type Nd-isotopic compositions, have LREE-depleted trace element pattern and sodium concentrations in cpx of up to 0.82 wt% [52]. Although these values are less than half of the concentrations observed at Lena Trough, they suggest that sodic metasomatism may occur at spreading centers.

Although a passive exhumation origin is plausible in the case of Lena Trough, an active melting scenario is more likely. It requires that sodic metasomatism can occur here and elsewhere in the oceanic lithosphere.

## 5. Conclusions

1. Serpentinized spinel peridotites were dredged from sediment-free basement highs along the previously unstudied Lena Trough. The primary mineral compositions of these outcropping melting residues are similar to other RAPs, except for sodium in cpx, which is transitional between continental and oceanic mantle.
2. The Lena Trough peridotites are devoid of magmatic veins and plagioclase and most samples have light REE-depleted trace element patterns typical of oceanic melting residues. Degrees of melting estimated from the cpx REE patterns of these 'normal' samples range between 7 and 10%.
3. The middle- to heavy REE characteristics indicate that roughly half of the melt extraction occurred under garnet-facies conditions. This requires deep initial melting, possibly caused by the presence of water (lowering the peridotite solidus) or a high mantle potential temperature.
4. Low overall degrees of melting suggest deep cessation of melting, most likely influenced by the vicinity to cold lithospheric mantle and the extremely slow effective spreading rate caused by the highly oblique opening of Lena Trough.
5. Sodium concentrations in cpx are too high to be explained by partial melting and not consistent with LREE-depleted residual cpx. Neither refertilization by a melt, nor simple diffusive processes can generate the pervasive fractionation of Na from the LREE. Cryptic sodic metasomatism, generally assumed to be restricted to the subcontinental mantle, must have occurred after partial melting.
6. No constraints are presently available for the absolute timing of melting and metasomatism. The Lena Trough peridotites could represent a fragment of subcontinental lithospheric mantle, tectonically exhumed without significant chemical modification. This implies that the trace element signatures in Lena Trough and possibly some other abyssal peridotite cpx REE systematics might point to an 'old' or inherited melt extraction event, not related to

melting underneath the present ridge. Alternatively, the opening of Lena Trough did lead to partial melting of the upwelling mantle, followed by sodic metasomatism in an oceanic environment.

## Acknowledgements

## References

[1] A. Miyashiro, F. Shido, M. Ewing, Composition and origin of serpentinites from the Mid-Atlantic ridge near 24 degrees and 30 degrees north latitude, Contrib. Mineral. Petrol. 23 (1969) 117–127.

[2] F. Aumento, H. Loubat, The Mid-Atlantic Ridge near 45°N. Serpentinized ultramafic intrusions, Can. J. Earth Sci. 8 (1971) 631–663.

[3] B.E. Tucholke, J. Lin, M.C. Kleinrock, Megamullions and mullion structure defining oceanic metamorphic core complexes on the Mid-Atlantic Ridge, J. Geophys. Res. 103 (1998) 9857–9866.

[4] J.R. Cann, D.K. Blackman, D. Smith, E. McAllister, B. Janssen, S. Mello, E. Avgerinos, A.R. Pascoe, J. Escartin, Corrugated slip surfaces formed at ridge-transform intersections on the Mid-Atlantic Ridge, Nature 385 (1997) 329–332.

[5] M. Cannat, C. Mevel, M. Maia, C. Deplus, C. Durand, P. Gente, P. Agrinier, A. Belarouchi, G. Dubuisson, E. Humler, J. Reynolds, Thin crust, ultramafic exposures, and rugged faulting patterns at the Mid-Atlantic Ridge (22 degrees-24 degrees N), Geology 23 (1995) 49–52.

[6] M. Cannat, Emplacement of mantle rocks in the seafloor at mid-ocean ridges, J. Geophys. Res. 98 (1993) 4163–4172.

[7] E. Bonatti, G. Ottonello, P. Hamlyn, Peridotites from the island Zabargad (St. John), Red Sea petrology and geochemistry, J. Geophys. Res. 91 (1986) 599–631.

[8] J. Kornprobst, A. Tabit, Plagioclase-bearing ultramafic tectonites from the Galicia margin (Leg 103, Site 637); comparison of their origin and evolution with low-pressure ultramafic bodies in Western Europe, Proc. ODP Sci. Res. 103 (1988) 253–268.

[9] H.J.B. Dick, J. Lin, H. Schouten, Ultraslow spreading - a new class of ocean ridge, Nature, 2003 (in press).

[10] E. Hellebrand, J.E. Snow, C.W. Devey, K.M. Haase, A.W. Hofmann, Cumulate trace element signature in diopsides from plagioclase peridotites from Molloy Ridge, MAR 79°N, in: AGU Spring Meeting, EOS Trans. AGU, Boston, MA, 1998.

[11] R.B. Whitmarsh, G. Manatschal, T.A. Minshull, Evolution of magma-poor continental margins from rifting to seafloor spreading, Nature 413 (2001) 150–154.

[12] D. Chian, K.E. Louden, T.A. Minshull, Deep structure of the ocean-continent transition in the southern Iberia Abyssal Plain from seismic refraction profiles: Ocean Drilling Program (Leg 149 and 173) transect, J. Geophys. Res. 104 (1999) 7443–7462.

[13] T.J. Reston, C.M. Krawczyk, D. Kläschen, The S reflector west of Galicia (Spain): evidence for detachment faulting during continental breakup from prestack depth migration, J. Geophys. Res. 101 (1996) 8075–8091.

[14] J. Hermann, O. Müntener, V. Trommsdorff, W. Hansmann, G.B. Piccardo, Fossil crust-to-mantle transition, Val Malenco (Italian Alps), J. Geophys. Res. 102 (1997) 20123–20132.

[15] O. Müntener, J. Hermann, The role of lower crust and continental upper mantle during formation of non-volcanic passive continental margins: evidence from the Alps, in: R.C.L. Wilson, R.B. Whitmarsh, B. Taylor, N. Froitzheim (Eds.), Non-volcanic Rifting of Continental Margins, Geol. Soc. Spec. Publ. 187, London, 2001, pp. 267–288.

[16] E. Hellebrand, Petrology, in: W. Jokat (Ed.), The Expedition ARKTIS-XV/2 of 'Polarstern' in 1999, Rep. Pol. Res. 368, 2000, pp. 59–70.

[17] W. Jokat, The sediment distribution below the North Greenland continental margin and the adjacent Lena Trough, Polarforschung 68 (1998) 71–82.

[18] P.J. Michael, C.H. Langmuir, H.J.B. Dick, J.E. Snow, S.L. Goldstein, D.W. Graham, K. Lehnert, G. Kurras, R. Mühe, H.N. Edmonds, Magmatic and amagmatic seafloor spreading at the slowest mid-ocean ridge: Gakkel Ridge, Arctic Ocean, Nature 423 (2003) 956–965.

[19] H. Brueckner, M. Elhadad, B. Hamelin, S. Hemmings, A. Kroener, L. Reisberg, M. Seyler, A Pan-African origin and uplift for the gneisses and peridotites of Zabargad-Island, Red Sea - A Nd, Sr, Pb, and Os isotope study, J. Geophys. Res. 100 (1995) 22283–22297.

[20] J.E. Snow, G. Schmidt, Proterozoic melting in the northern peridotite Massif, Zabargad Island: Os isotopic evidence, Terra Nova 11 (1999) 45–50.

[21] E. Rampone, A.W. Hofmann, I. Raczek, Isotopic contrasts within the Internal Liguride ophiolite (N. Italy): the lack of a genetic mantle-crust link, Earth Planet. Sci. Lett. 163 (1998) 175–189.

[22] R.S. White, T.A. Minshull, M.J. Bickle, C.J. Robinson, Melt generation at very slow-spreading oceanic ridges: Constraints from geochemical and geophysical data, J. Petrol. 42 (2001) 1171–1196.

[23] R. Mühe, E. Hellebrand, J.E. Snow, Petrology and geochemistry of Lena Trough alkali basalts, Chem. Geol., in prep.

[24] E. Hellebrand, J.E. Snow, P. Hoppe, A.W. Hofmann, Garnet-field melting and late-stage refertilization in 'residual' abyssal peridotites from the Central Indian Ridge, J. Petrol. 43 (2002) 2305–2338.

[25] K.P. Jochum, D.B. Dingwell, A. Rocholl, B. Stoll, A.W. Hofmann, S. Becker, A. Besmehn, D. Bessette, H. Dietze, P. Dulski, J. Erzinger, E. Hellebrand, P. Hoppe, I. Horn, K. Janssens, G.A. Jenner, M. Klein, W.F. McDonough, M. Maetz, K. Mezger, C. Münker, I.K. Nikogosian, C. Pickhardt, I. Raczek, D. Rhede, H.M. Seufert, S.G. Simakin, A.V. Sobolev, B. Spettel, S. Straub, L. Vincze, A. Wallianos, G. Weckwerth, S. Weyer, D. Wolf, M. Zimmer, The preparation and preliminary characterisation of eight geological MPI-DING standard reference glasses for in-situ microanalysis, Geost. Newslett. 24 (2000) 87–133.

[26] M. Seyler, E. Bonatti, Regional-scale melt-rock interaction in lherzolitic mantle in the Romanche fracture zone (Atlantic Ocean), Earth Planet. Sci. Lett. 146 (1997) 273–287.

[27] K.T.M. Johnson, H.J.B. Dick, N. Shimizu, Melting in the oceanic upper mantle; an ion microprobe study of diopsides in abyssal peridotites, J. Geophys. Res. 95 (1990) 2661–2678.

[28] K.T.M. Johnson, H.J.B. Dick, Open system melting and temporal and spatial variation of peridotite and basalt at the Atlantis II fracture zone, J. Geophys. Res. 97 (1992) 9219–9241.

[29] H.J.B. Dick, J.H. Natland, Late-stage melt evolution and transport in the shallow mantle beneath the East Pacific Rise, Proc. ODP Sci. Res. 147 (1996) 103–134.

[30] K. Ross, D. Elthon, Extreme incompatible trace-element depletion of diopside in residual mantle from south of the Kane F.Z., Proc. ODP Sci. Res. 153 (1997) 277–284.

[31] E. Hellebrand, J.E. Snow, H.J.B. Dick, A.W. Hofmann, Coupled major and trace elements as indicators of the extent of melting in mid-ocean ridge peridotites, Nature 410 (2001) 677–681.

[32] H.J.B. Dick, T. Bullen, Chromian spinel as a petrogenetic indicator in abyssal and alpine-type peridotites and spatially associated lavas, Contrib. Mineral. Petrol. 86 (1984) 54–76.

[33] J.A.C. Robinson, B. Wood, The depth of the spinel to garnet transition at the peridotite solidus, Earth Planet. Sci. Lett. 164 (1998) 277–284.

[34] C.H. Langmuir, E.M. Klein, T. Plank, Petrologic systematics of mid-ocean ridge basalts: constraints on melt generation beneath ocean ridges, in: J. Phipps-Morgan, D.K. Blackman, J.M. Sinton (Eds.), Mantle Flow and Melt Generation at Mid-ocean Ridges, AGU Monogr. 71, 1992, pp. 183–280.

[35] D. McKenzie, M.J. Bickle, The volume and composition of melt generated by extension of the lithosphere, J. Petrol. 29 (1988) 625–679.

[36] D.H. Green, Experimental melting studies on a model upper mantle composition at high-pressure under water-saturated and water-undersaturated conditions, Earth Planet. Sci. Lett. 19 (1973) 37–53.

[37] E. Bonatti, M. Ligi, D. Brunelli, A. Cipriani, P. Fabretti, V. Ferrante, L. Gasperini, L. Ottolini, Mantle thermal pulses below the Mid-Atlantic Ridge and temporal variations in the formation of oceanic lithosphere, Nature 423 (2003) 499–505.

[38] K. Niida, Mineralogy of MARK peridotites: replacement through magma channeling examined from Hole 920D, MARK area, Proc. ODP Sci. Res. 153 (1997) 243–264.

[39] G. Suhr, E. Hellebrand, J.E. Snow, H. Seck, A.W. Hofmann, Significance of large, refractory dunite bodies in the upper mantle of the Bay of Islands Ophiolite, Geochem. Geophys. Geosyst. 4 (2003) 8605, doi: 10.1029/2001GC000277.

[40] P.B. Kelemen, N. Shimizu, V.J.M. Salters, Extraction of mid-ocean-ridge basalt from the upwelling mantle by focused flow of melt in dunite channels, Nature 375 (1995) 747–753.

[41] E.M. Klein, C.H. Langmuir, Global correlations of ocean ridge basalts with axial depth and crustal thickness, J. Geophys. Res. 92 (1987) 8089–8115.

[42] D. Elthon, Chemical trends in abyssal peridotites; refertilization of depleted suboceanic mantle, J. Geophys. Res. 97 (1992) 9015–9025.

[43] P.D. Asimow, A model that reconciles major- and trace-element data from abyssal peridotites, Earth Planet. Sci. Lett. 169 (1999) 303–319.

[44] M.B. Baker, J.R. Beckett, The origin of abyssal peridotites: a reinterpretation of constraints based on primary bulk compositions, Earth Planet. Sci. Lett. 171 (1999) 49–61.

[45] H.J.B. Dick, R.L. Fisher, W.B. Bryan, Mineralogic variability of the uppermost mantle along mid-ocean ridges, Earth Planet. Sci. Lett. 69 (1984) 88–106.

[46] H.J.B. Dick, Abyssal peridotites, very slow spreading ridges and ocean ridge magmatism, Geol. Soc. Spec. Publ. 42 (1989) 71–105.

[47] R.J. Kinzler, T.L. Grove, Primary magmas of mid-ocean ridge basalts; 1, Experiments and methods, J. Geophys. Res. 97 (1992) 6885–6906.

[48] J. Blundy, T.J. Falloon, B. Wood, J.A. Dalton, Sodium partitioning between clinopyroxene and silicate melt, J. Geophys. Res. 100 (1995) 15501–15515.

[49] J. Blundy, J.A.C. Robinson, B. Wood, Heavy REE are compatible in clinopyroxene on the spinel lherzolite solidus, Earth Planet. Sci. Lett. 160 (1998) 493–504.

[50] C.C. Lundstrom, Rapid diffusive infiltration of sodium into partially molten peridotite, Nature 403 (2000) 527–530.

[51] J.A. van Orman, T.L. Grove, N. Shimizu, Rare earth element diffusion in diopside: influence of temperature, pressure, and ionic radius, and an elastic model for diffusion in silicates, Contrib. Mineral. Petrol. 141 (2001) 687–703.

[52] V.J.M. Salters, H.J.B. Dick, Mineralogy of the mid-ocean-ridge basalt source from neodymium isotopic composition of abyssal peridotites, Nature 418 (2002) 68–72.

[53] M. Seyler, M. Cannat, C. Mevel, Evidence for major-element heterogeneity in the mantle source of abyssal peridotites from the Southwest Indian Ridge (52° to 68°E), Geochem. Geophys. Geosyst. 4 (2003) 9101, doi: 10.1029/2002GC000305.

[54] E. Bonatti, P.J. Michael, Mantle peridotites from continental rifts to ocean basins to subduction zones, Earth Planet. Sci. Lett. 91 (1989) 297–311.

[55] J.E. Snow, S.R. Hart, H.J.B. Dick, Nd and Sr isotope evidence linking mid-ocean-ridge basalts and abyssal peridotites, Nature 371 (1994) 57–60.

[56] I. Ghose, M. Cannat, M. Seyler, Transform fault effect on mantle melting in the MARK area (Mid-Atlantic Ridge south of the Kane transform), Geology 24 (1996) 1139–1142.

[57] L. Beccaluva, G. Bianchini, M. Coltorti, W.T. Perkins, F. Siena, C. Vaccaro, M. Wilson, Multistage evolution of the European lithospheric mantle: new evidence from Sardinian peridotite xenoliths, Contrib. Mineral. Petrol. 142 (2001) 284–297.

[58] D. Smith, Insights into the evolution of the uppermost continental mantle from xenolith localities on and near the Colorado plateau and regional comparisons, J. Geophys. Res. 105 (2000) 16769–16781.

[59] U. Wiechert, D.A. Ionov, K.H. Wedepohl, Spinel peridotite xenoliths from the Atsagin-Dush volcano, Dariganga lava plateau, Mongolia: a record of partial melting and cryptic metasomatism in the upper mantle, Contrib. Mineral. Petrol. 126 (1997) 345–364.

[60] G. Witt-Eickschen, U. Kramm, Mantle upwelling and metasomatism beneath central Europe: geochemical and isotopic constraints from mantle xenoliths from the Rhön (Germany), J. Petrol. 38 (1997) 479–493.

[61] X. Xu, S. O'Reilly, W. Griffin, X. Zhou, Genesis of young lithospheric mantle in southeastern China: an LAM-ICPMS trace element study, J. Petrol. 41 (2000) 111–148.

[62] S. Charpentier, La zone de transition continent-ocean de la marge continentale passive ouest-iberique: etudes petrologique et geochimique des roches magmatiques et mantelliques, Ph.D. Thesis, Université Blaise Pascal, 2000.

[63] E. Anders, N. Grevesse, Abundances of the elements: meteoric and solar, Geochim. Cosmochim. Acta 53 (1989) 197–214.

[64] G.T.R. Droop, A general equation for estimating $Fe^{3+}$ concentrations in ferromagnesian silicates and oxides from microprobe analyses, using stochiometric criteria, Min. Mag. 51 (1987) 431–435.